An Eulerian photochemical model for tropospheric ozone over the tropics

S. B. Debaje* and D. B. Jadhav
Indian Institute of Tropical Meteorology, Pune 411 008, India

A time-dependent Eulerian photochemical model for the highly reactive tropospheric trace species is formulated to gain insight into the observed trace species (ozone, NOx, PAN, HOx, etc.) over the tropics. In the present study, the model is designed to simulate a dirunal variation of surface ozone and vertical profile of the tropospheric ozone up to 15 km by considering the chemical and physical processes. The basis for this model is the mass balance of the concerned species (for example, ozone in this study) and it is solved by using Euler's numerical techniques assuming quasi steady state approximation (QSSA) as suggested by Hov[1]. The various terms like advection, turbulent diffusion, chemical transformations, emission and removal in mass balance equation can be solved independently. Therefore, in this study, emphasis is on the chemistry of the mass balance equation of tropospheric ozone. The model results are compared with ozone measurements made at Pune. The simulated ozone concentrations for clear sky agree within less than 20% differences except for monsoon season (cloudy days). The high tropospheric ozone observed usually in March (summer season) is shifted to monsoon season in model results. This shift in ozone is due to the neglect of the impact of cloud and aqueous phase processes on tropospheric ozone production in the model.

MATHEMATICAL models are needed to study the highly reactive tropospheric trace species as their data are sparse and difficult to measure. These increasing highly reactive trace species (for example, tropospheric ozone (O_3), nitrogen dioxide (NO_2), nitric oxide (NO), peroxyacetyl nitrate (PAN) and reactive hydrocarbons) are mainly responsible for adverse impact on our biosphere. Predictions from mathematical models provide the means to assess the response of these highly reactive tropospheric trace species on future changes in the environment. Models can also be used to study the effect of an increase or decrease in the emissions of the highly reactive species on photochemical processes.

The Eulerian photochemical model is designed to simulate the concentrations of chemically highly reactive tropospheric trace species by simulating the physical and chemical processes in the troposphere. The chemistry and transport parts of the mass balance equation can be solved independently[1]. Therefore, the main emphasis is on an accurate description of the chemistry of the mass balance equation in this study.

The development and validation of the model are presented in three parts: (i) Formulation of the model; (ii) Inventory of trace species emissions; and (iii) Evaluation of the model.

The formulation of a model for predicting the dynamic behaviour of a highly chemically reactive tropospheric trace species in an urban atmosphere is studied. The basis for the model is the mass balance equation of the concerned highly reactive tropospheric trace species. This equation represents a mass balance in which all of the relevant emissions, transport, diffusion, chemical transformations and removal processes are expressed in mathematical terms as follows:

$$\begin{aligned} \partial c_i/\partial t = &- \partial(uc_i)/\partial x - \partial(vc_i)/\partial y - \partial(wc_i)/\partial z \\ &+ \partial K_H/\partial x\, \partial c_i/\partial x + \partial K_H/\partial y\, \partial c_i/\partial y \\ &+ \partial K_V/\partial z\, \partial c_i/\partial z + R_i + S_i + L_i, \end{aligned} \quad (1)$$

where c_i represents the concentration of species i and is a function of space (x, y, z) and time (t). Subscript i denotes the number of species ($i = 1, 2, \ldots, n$; where n is the number of species to be studied) simulated in the model. For simplicity in the chemical scheme the single species (ozone) is studied by putting $n = 1$ in the model eq. (1).

The other terms in eq. (1) are:
u, v, w are meridional and zonal wind speed components;
K_H, K_V are horizontal and vertical turbulent diffusion coefficients;
R_i is net rate of production of species i by chemical transformations;
S_i is emission rate of species i, and L_i is net rate of removal of species i by surface uptake processes (dry and wet deposition).

Equation (1) is integrated forward in time using an Euler numerical technique[1]. Numerical solution of eq. (1) requires specification of initial conditions, together with time- and space-resolved descriptions of meteorology and emissions at the grid point.

Equation (1) can be simplified, for the study of ozone initially by putting $n = 1$ for a single cell and applying the following assumptions:
(i) advection term is neglected; (ii) concentration of the species is uniform in the grid, i.e. turbulent diffusion is neglected; and (iii) emission and deposition terms are neglected.

Then, eq. (1) reduces to

$$\partial c_i/\partial t = R_i(\{P_K\}t, T) \quad (2)$$

where R_i is the net generation term of the ozone (balance of chemical production and destruction) and is a function of space and time. In eq. (2), $\{P_K\}$ stands for a detailed photochemical mechanism, including all the relevant species participating in the O_3 generation and destruction, and is a function of space, time, temperature (T) and solar zenith angle (z).

*For correspondence. (e-mail: debaje@tropnet.ernet.in)

The chemistry in eq. (2) is defined to be as simple as possible so that the number of equations (and hence number of species) could be kept at a minimum. Chemical transformation processes are known to be difficult to handle numerically. The set of reactions used is a simplified version of a chemical scheme for the investigation of a chemical transformation of species (O_3) in the troposphere[2]. The condensed chemical scheme omits parallel chemical paths and concentrates on generic aspects of the chemical interaction between the highly reactive trace species. The chemistry is driven by two forces, namely solar radiation and sources of highly reactive trace species. There are two major sunlight-induced photolytic processes in the troposphere, one is the photolysis of NO_2 and other is production of O_3. The former produces NO and O_3 in the troposphere. The chemical scheme used in eq. (2) is given in Table 1.

Equation (1) can be split into several parts (chemistry part, diffusion part, transport part, emission part and removal part) and each part is integrated separately at each time step[1]. The main principles that are applied in the integration of the chemical part are based on a quasi steady state approximation (QSSA). In QSSA it is assumed that rate of production and destruction of species in eq. (2) are constant over a time step interval for a given species while integrating. The integration of eq. (2) is performed forward in time with a time step of 1 hour using Euler's numerical techniques.

The model requires hourly input data of NO, NO_2, J_{NO_2} and temperature (T) for simulation of O_3 concentration in eq. (2). The other species are kept constant while integrating eq. (2). The hourly averaged surface diurnal variations of NO_x input data for diurnal O_3 simulation at Pune latitude are derived from Logan *et al.*[5] and Subbaraya *et al.*[6]. The reaction rate constant (k) and the NO_2 photodissociation rate (J_{NO_2}) are calculated by using diurnal variation in temperature and solar zenith angle, respectively at Pune latitude as per the chemical scheme used in Table 1. The diurnal variation in temperature data is used from Tiwari and Peshin[7] and vertical temperature profile is taken from Mani and Sreedharan[8] for Pune (19°N). The vertical NO and NO_2 profiles are derived from Logan *et al.*[5] to simulate the vertical O_3 profile at Pune. The photodissociation rate of NO_2 is calculated at 19°N using solar zenith angle for local noon (1200 h) while simulating vertical O_3 profile in the troposphere. Annual variations of tropospheric ozone are simulated at an interval of 15 days by varying the photodissociation rate of NO_2 and using average vertical NO, NO_2 and temperature profiles at Pune.

The photodissociation rate of NO_2 is a function of altitude and it increases with altitude as actinic flux increases[9,10]. To consider this increase in J_{NO_2} with altitude, the troposphere is divided into three parts, surface–5 km, 5–10 km and 10–15 km. J_{NO_2} calculated at surface is kept constant for surface–5 km. J_{NO_2} is increased by 2.5% of surface value for 5–10 km and by 5% of surface value for 10–15 km as the actinic flux profile for a cloudless atmosphere linearly increases[10]. Input data to the model were adjusted to avoid the appearance of negative concentrations and as closely as possible to match the initial field conditions for the seasons at Pune. In view of the simplicity of the model, the contribution from natural and anthropogenic hydrocarbons in O_3 formation is not included. But it is possible to include natural hydrocarbons like isoprene and anthropogenic hydrocarbons which have high maximum incremental reactivity (MIR) value as suggested by Carter[11] regarding ozone forming potential (for example, MIR of isoprene is 9.1 g O_3/g isoprene).

The reliability of any model can be evaluated by comparisons of simulated results with measurements. The comparisons were carried out by using O_3 measurements made by Tiwari and Peshin[7] (averaged on an hourly basis) on a time scale of one day with simulated O_3 by simulating the chemical scheme given in Table 1. Comparisons of simulated vertical O_3 profiles were carried out with measured vertical O_3 profile by Mani and Sreedharan[8]. In this study a primary attempt is made to simulate the chemistry part of the atmospheric processes in the mass balance model eq. (1). It is important to simulate diurnal and vertical profile variations of the highly reactive trace species that participate in a photochemical reaction in the troposphere. For example, it is essential to determine correctly daily maxima of surface ozone concentrations (hourly averaged permissible limit is 80 parts per billion by volume (ppbv) as per World Health Organization (WHO) air quality guidelines) because ozone can have damaging effects on all living things[12].

Table 1. Chemical scheme used in the eq. (2)

$NO_2 + h\nu \rightarrow NO + O_3$ $J = 1.33 \times 10^{-2} \exp(-0.254 \sec(z))$	Tremmel (1992)	(R1)
$NO + O_3 \rightarrow NO_2 + O_2$ $k = 2.0 \times 10^{-12} \exp(-1370/T)$	Atkinson (1992)	(R2)
$O_3 + h\nu \rightarrow O(^1D) + O_2$ $J = 8.58 \times 10^{-4} \exp(-2.55 \sec(z))$	Tremmel (1992)	(R3)
$O(^1D) + O_2 + M \rightarrow O_3 + M$ $k = 1.82 \times 10^{-11} \exp(110/T)^{0.78}$ $+ 3.2 \times 10^{-11} \exp(70/T)^{0.21}$	DeMore *et al.* (1987)	(R4)
$O_3 + OH \rightarrow HO_2 + O_2$ $k = 1.6 \times 10^{-12} \exp(-940/T)$	DeMore *et al.* (1987)	(R5)
$O_3 + HO_2 \rightarrow OH + 2O_2$ $k = 1.1 \times 10^{-14} \exp(-500/T)$	DeMore *et al.* (1987)	(R6)
$NO + HO_2 \rightarrow NO_2 + OH$ $k = 3.7 \times 10^{-12} \exp(240/T)$	DeMore *et al.* (1987)	(R7)
$NO_2 + OH + M \rightarrow HNO_3 + M$ $k = 6.0 \times 10^{-11}$	Atkinson *et al.* (1992)	(R8)

$\sec(z) = 1/\cos(z)$, z is the local solar zenith angle; $\cos(z) = \cos(\text{LHA}) \cos(\text{LAT}) \cos(\text{DEC}) + \sin(\text{LAT}) \sin(\text{DEC})$, LHA = local angle of hour, which is 0° for local noon (1200 h) and increments by 15° for each hour from noon; LAT = latitude at Pune; DEC = sun declination; h is Planck's constant and ν is frequency of radiation; k is the first-order reaction rate constant; J is photolysis rate of the molecule is in (s^{-1}) unit. All reaction rate constants (k) in (cm^3 $molecule^{-1}$ s^{-1}) unit. All reaction rate constants used are from Schmidt *et al.*[3]. The cosine of the local solar zenith angle (z) is given by Brasseur and Solomon[4].

The model simulated results for diurnal ozone variation and vertical ozone profile concentrations are encouraging when compared with measurements made by Tiwari and Peshin[7] and Mani and Sreedharan[8] at Pune. All the results agree very well within less than 10 to 30% differences. These differences can be reduced sufficiently by choosing appropriate time steps to integrate eq. (2). In the present study a time step of 1 hour is taken for simulation of the model. To achieve good results, it is required to use accurate input data with high resolution, especially for NO and NO_2 which have very high ozone forming potential. In this sense the input data used in the model at present have less resolution. In spite of these difficulties, an attempt is made to simulate atmospheric processes (chemistry part) in the mathematical model eq. (2). The results can potentially be improved by refining the input data field (here, especially, the emission fields are important). Simulation for NO_2, NO, PAN and other trace species is also possible by adding appropriate chemical reactions which contribute in production and destruction of the species in the chemical scheme given in Table 1.

Figures 1 and 2 show the comparison of diurnal variation of ozone and vertical ozone profile concentration with measured ozone concentration in winter (January). The simulated results match very well with measurements. In Figure 1 simulated diurnal variation of ozone is compared with measurements made by Tiwari and Peshin[7] and Khemani *et al.*[13] at Pune. The diurnal variation of ozone in winter (January) shows maximum ozone concentration (more than 40 ppbv) around 1200 h and minimum concentration (less than 10 ppbv) before sunrise (0700 h) as observed by these workers. Simulated O_3 maxima follow O_3 measurements but simulated O_3 minima do not follow O_3 measurements. In Figure 1, O_3 values of Khemani *et al*. are more than the simulated values whereas O_3 values of Tiwari and Peshin are less than the simulated values. The important feature in our result is that simulated O_3 follows general diurnal features. This means that we are able to simulate diurnal variation pattern, maxima and minima of surface ozone up to a certain extent. The simulated surface ozone maxima around noon is better when compared with measurements than its minima in the morning. The morning minima of surface ozone is related to the complex night-time chemistry

of nitrate radical (NO_3). The NO_3 chemistry strongly depends upon ambient temperature and aqueous phase reactions. The chemical reactions of night-time chemistry of NO_3 for surface ozone destruction are not included in the present chemical scheme in the Table 1. Hence morning minima of simulated surface ozone does not compare well with measurements. The differences in simulated O_3 with measured O_3 by Tiwari and Peshin[7] and Khemani *et al*.[13] may be due to different measurement locations and different O_3 measuring techniques. The simulated vertical profile of ozone is compared with measured ozone profile by Mani and Sreedharan[8] in Figure 2. The simulated O_3 profile compares well with the measured profile. The simulated tropospheric O_3 maxima is at about 2 km whereas measured O_3 maxima is at the surface. The simulated and measured tropospheric O_3 minima are at about 15 km (below the local tropopause level) as observed by Mani and Sreedharan. The ozone level starts increasing above 15 km in the stratosphere.

Figure 3 shows the contour map of annual (1 to 365 days)

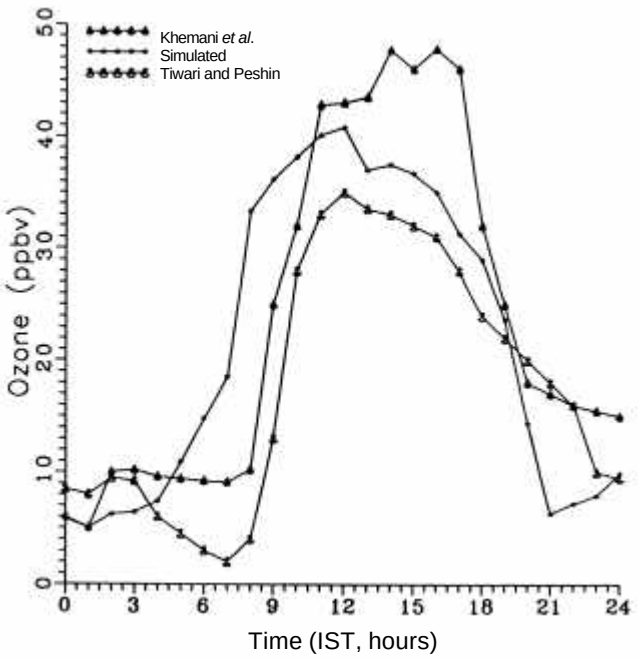

Figure 1. Diurnal variation of surface ozone in winter at Pune.

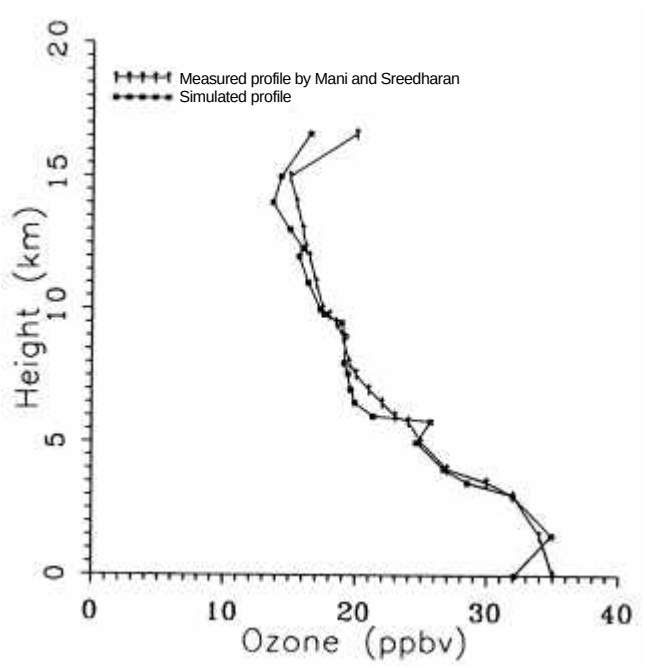

Figure 2. Tropospheric vertical profile of ozone in winter at Pune.

tropospheric ozone at Pune latitude simulated at an interval of 15 days (day number × 15 = day of the year) by varying value. The maximum O_3 concentration occurs at about 2 km and changes from day to day and from month to month. The highest tropospheric O_3 concentration observed from surface to 7 km occurs in June and the lowest in December–January. At altitudes of about 2–3 km and 6–7 km gradients (distance between two contour lines are less) of tropospheric O_3 are simulated and thereafter above 7 km the gradients are less (distance between two contour lines are more). During winter when temperatures fall, the thermal decomposition of ozone precursors (PAN and active hydrocarbons) decreases and their atmospheric lifetime increases. In this way more ozone precursors are accumulated as temperature decreases during winter. In March, temperatures start increasing due to high radiation and accumulated ozone precursors thermally decompose, producing more active radicals. This results in photochemical ozone processes which are more active producing more ozone in the month of March mostly when clear sky condition prevails. From April onwards, pre-monsoon cloud in the sky disturbs the photochemical ozone production processes in the troposphere resulting in less ozone production. This indicates that photochemical ozone production in the troposphere is active in March which is supported by measurements[7]. Figure 3 shows that the maximum O_3 concentration occurs at about 2–3 km during June instead of March.

Model eq. (2) is simulated for the vertical O_3 profile without considering the cloud effect. The cloud plays a very important role in tropospheric O_3 formation during the monsoon season. The photodissociation rate of NO_2 (reaction R1 in Table 1) is proportional to the actinic flux[10] and it is the only reaction which produces ozone in the troposphere. The actinic flux deals with the energy that is incident on a molecule. In the lowest parts of the troposphere the effect of the cloud on the actinic flux can be very strong. The actinic flux in-cloud, above and below clouds depends on the cloud optical thickness and solar zenith angle. The cloud optical thickness depends on origin of the cloud, (i.e. marine cloud or continental cloud). The marine cloud has high optical thickness due to the presence of more small particles than continental cloud. The winds are south-westerly in the monsoon season and cloud mainly transported to Pune originate from the Arabian Sea. These clouds have high optical thickness which reduces actinic flux considerably in the troposphere at Pune. This reduction in actinic flux decreases photodissociation rate of NO_2 and results in less O_3 production. Thus the cloud plays a dominant role in tropospheric O_3 formation by dissociation of NO_2 molecule.

In another study by Jonson and Isaksen[14], the impact of cloud chemistry on tropospheric ozone chemistry has shown that the loss of ozone in an aqueous phase, with pronounced reduction in ozone levels by about 10 to 30% in the troposphere are due to these processes (Reaction R8 in Table 1). These processes affect ozone in two ways: they reduce the gas-phase concentration of the species involved (precursors) in ozone production, and they provide a source for compounds interacting with ozone in the aqueous phase. This fact supports the minimum ozone measurements in August by Mani and Sreedharan[8].

Equation (2) is simulated without cloud effect and aqueous phase reactions, hence the tropospheric O_3 maxima in Figure 3 is seen at height of about 2–3 km during monsoon season (August) instead of in the summer season (March). If 10, 20 and 30% ozone are subtracted (as per the study of Jonson and Isaksen) from simulated ozone for winter to summer, post-monsoon and monsoon season, respectively, then minimum ozone will be found in monsoon season (August) instead of December–January. The annual amount of cloud data is used from Nighut[15]. This brings the

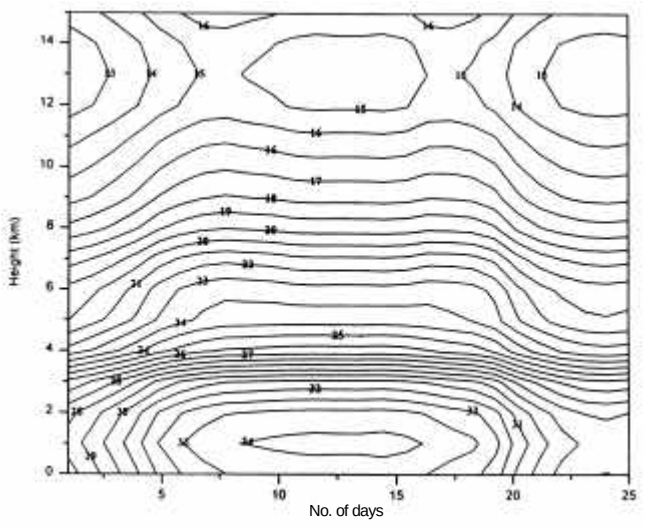

Figure 3. Contour map of ozone (ppbv) without cloud effect at Pune.

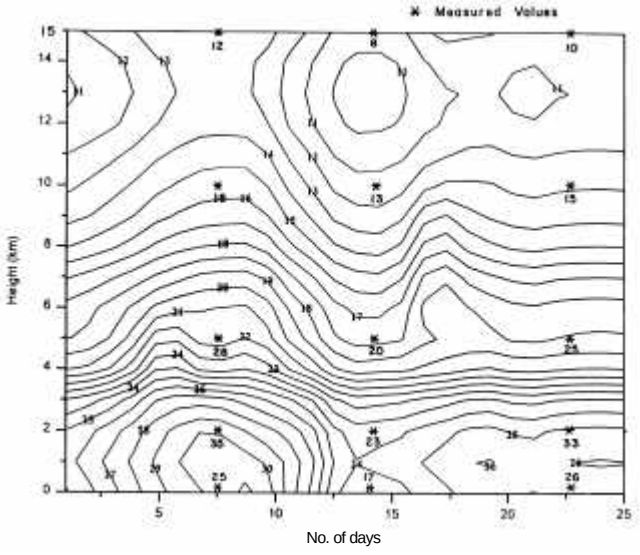

Figure 4. Contour map of ozone (ppbv) with cloud effect at Pune.

Table 2. Comparison of simulated vertical ozone (ppbv) profile with and without cloud impact with the mean profiles of soundings made at Pune[8]

Height (km)	Winter			Summer			Monsoon			Post–monsoon		
	M	S	*	M	S	*	M	S	***	M	S	**
Surface	23	27	24	26	31	28	15	32	22	25	30	24
2	28	31	28	29	35	31	23	34	24	23	34	27
5	20	20	20	26	24	26	20	24	17	20	23	20
10	13	15	14	12	15	13	9	16	11	13	15	13
15	12	14	13	13	13	13	7	14	10	11	14	13

M, measured ozone value; and S, simulated ozone without cloud effect.
∗, simulated ozone with cloud effect for different seasons,
∗, simulated ozone value is reduced by 10% in winter and summer season,
∗∗, simulated ozone value is reduced by 20% in post-monsoon season,
∗∗∗, simulated ozone value is reduced by 30% in monsoon season.
The annual amount of cloud data are used from Nighut[15].
Source: Nighut[15].

simulated ozone results in better agreement with measurements made by Mani and Sreedharan. The physical removal process of species (washout by rain) is also dominant during monsoon season and is not considered while simulating O_3 profile (Reaction R8 in Table 1). This results in shift of tropospheric O_3 maxima from summer to monsoon. The results will improve if cloud effect and removal processes are considered while simulating O_3 in eq. (2).

Table 2 compares simulated vertical O_3 profile with and without cloud impact for some selected heights (surface, 2, 5, 10, 15 km) with the mean profile of soundings made at Pune during the four main seasons, winter (November–February), summer (March–May), monsoon (June–August) and post-monsoon (September–October). For comparison it is considered that December 15 is representative of winter, March 15 is representative of summer, August 15 is representative of monsoon and October 15 is representative of post-monsoon season.

From Table 2 it is seen that measured O_3 concentrations, simulated O_3 without cloud impact for winter, summer and post-monsoon seasons are comparable within less than 10 to 30% differences whereas during monsoon season they are not comparable. The reason for this is that the cloud effect and removal processes are more pronounced in the monsoon season. After considering the cloud impact and aqueous phase processes, simulated results for tropospheric ozone agree well with measurements (Table 2 columns with * marks and Figure 4). If cloud effect is incorporated in the result then simulated ozone is comparable with measurements made by Mani and Sreedharan. Figure 4 shows that simulated maximum ozone in March and minimum in August compare well with measurements. It also reveals that ozone contour height increases in March whereas it decreases in August in the troposphere. These variations are expected in the troposphere considering the ozone formation and destruction mechanism. The present study helps to understand the mathematical modelling response of photochemical processes to tropospheric ozone and its precursor level in the troposphere over the Indian region. The proposed chemical scheme used in the model will also be tested for other highly reactive species like NO, NO_2 and PAN in the Indian sub-continent in the near future.

1. Hov, *Atmos. Environ.*, 1983, **17**, 535.
2. Zimmermann, J. and Poppe, D., *Atmos. Environ.*, 1993, **17**, 141.
3. Schmidt, R. W. H., Slemr, F. and Schurath, V., *Atmos. Environ.*, 1998, **32**, 1203.
4. Brasseur, G. and Solomon, S., *Aeronomy of the Middle Atmosphere*, D. Reidel Publishing Co., Holland, 1984, p. 104.
5. Logan, J. A., Prathor, M. J., Wofsy, S. C. and McElroy, M. B., *J. Geophys. Res.*, 1981, **86**, 7210.
6. Subbaraya, B. H., Rao, D. P., Desai, P. S., Manikiam, B. and Rajaratnam, P., Scientific Results from Indian Space Research Organization, Geosphere Biosphere Programme, Bangalore, India, 1998, p. 17.
7. Tiwari, V. S. and Peshin, S., *Mausam*, 1995, **46**, 155.
8. Mani, A. and Sreedharan, C. R., *Pure Appl. Geophys.*, 1973, **106–108 V–VII**, 1180.
9. Seinfeld, J. H., *Atmospheric Chemistry and Physics of Air Pollution*, Wiley, New York, 1986.
10. Weele, M. V. and Duynkerke, P. G., *J. Atmos. Chem.*, 1993, **16**, 231.
11. Carter, W. P. L., *J. Air Waste Manage. Assoc.*, 1994, **44**, 881.
12. Brauer, M. and Brook J. R., *Atmos. Environ.*, 1997, **31**, 2113.
13. Khemani, L. T., Momin, G. A., Rao, P. S. P., Vijaykumar, R. and Safai, P. D., *Atmos. Environ.*, 1995, **29**, 2021.
14. Jonson, J. E. and Isaksen, I. S. A., *J. Atmos. Chem.*, 1993, **16**, 99.
15. Nighut, D. N., Ph D thesis, University of Pune, 1997.

ACKNOWLEDGEMENTS. We thank Dr G. B. Pant, Director, Indian Institute of Tropical Meteorology, Pune for his keen interest in this study. We are grateful to the referees for their helpful comments and suggestions.

Received 18 January 1999; revised accepted 5 October 1999

Engineering resistance against physalis mottle tymovirus by expression of the coat protein and 3′ noncoding region

C. T. Ranjith-Kumar*, M. Manoharan†, S. Krishna Prasad*, Shoba Cherian*, M. Umashankar*, G. Lakshmi Sita† and H. S. Savithri*,‡

*Department of Biochemistry, Indian Institute of Science, Bangalore 560 012, India
†Department of Microbiology and Cell Biology, Indian Institute of Science, Bangalore 560 012, India

A 748 nucleotides cDNA fragment corresponding to the 3′ terminal of physalis mottle virus, PhMV (formerly known as belladonna mottle virus) (#Y16104) genomic RNA encompassing the tymobox, coat protein ORF and 3′ noncoding region was cloned into the binary vector pKYLX 71 35 S^2 and introduced into *N. tabacum* cv. Havana plants using *Agrobacterium*-mediated transformation. The R0 transgenic plants showed accumulation of coat protein which self-assembled into capsids *in vivo*. The transgenic R1 and R2 plants showed delay in symptom expression and virus accumulation upon challenge with PhMV. 55 and 65% of the plants showed no detectable symptoms in the R1 and R2 transgenic plants respectively, when challenged with 10 µg/ml virus. Further, no detectable symptoms were observed in 75% and 25% of the R1 and R2 transgenic plants respectively, after 50 days of post infection when challenged with 10 µg/ml RNA. Thus the expression of PhMV coat protein and 3′ noncoding sequence confers a high level of resistance against PhMV infection.

SANFORD and Johnston[1] suggested that engineered resistance to insect, fungal and viral parasites of plants could be achieved by utilizing portions of the pathogen's own genome. This concept of pathogen-derived resistance was first demonstrated in transgenic tobacco plants expressing the coat protein gene of tobacco mosaic tobamovirus (TMV)[2]. Since then, genetically engineered resistance has been reported for a number of plant viruses involving virus-derived genes or genome fragments[3–6].

Physalis mottle tymovirus (PhMV) (formerly known as belladonna mottle virus) belongs to the tymovirus group of plant viruses[7]. It consists of a 6.67 kb RNA genome (gene bank #Y16104)[8] encapsidated in a protein shell of 180 identical subunits (MW 20 kDa). The first attempt to generate transgenic plants resistant to tymovirus was made by Zaccomer *et al.*[9] by introducing 3′ terminal 100 nucleotides of turnip yellow mosaic tymovirus (TYMV) genome into rapeseed plants. These transgenic plants expressing the sense transcripts showed partial protection against TYMV infection, which was overcome when the inoculum concentration was increased. It was proposed that the competition of the sense RNA transgene transcript with the viral RNA for the viral replicase conferred resistance to viral infection in these plants[9].

In an earlier study, using an *in vivo* protoplast assay system we have shown that effective inhibition of virus multiplication was observed when protoplasts were coinoculated with PhMV genomic RNA (gRNA) and a transcript corresponding to 748 nucleotides from the 3′ end of the genome[10]. This 3′ terminal sequence encompassed a conserved 16 nucleotide sequence called the tymobox[11] upstream of the coat protein (CP) open reading frame (ORF), the CP gene and the entire 3′ noncoding (NC) region of PhMV RNA. In order to assess whether the expression of CP and NC would confer resistance to virus infection, we have developed transgenic tobacco plants by introducing the 3′ terminal 748 nucleotides of PhMV into the *N. tabaccum* genome. The transgenic plants not only showed expression of the CP gene but also exhibited a high level of resistance against intact virus as well as RNA infection in the R1 and R2 generation plants.

[α-^{32}P]dATP (3000 Ci/mmol) was obtained from Amersham International. Restriction endonucleases and DNA modification enzymes were purchased from New England Biolabs and Amersham International. All other chemicals were of analytical grade. The oligonucleotide primers were purchased from Bangalore Genei Pvt. Ltd, India.

PhMV was maintained on the systemic host *N. tabacum* cv. Havana. Transformation and regeneration experiments were also performed using the same host. PhMV was purified as described earlier[12] and gRNA was isolated according to Jacob *et al.*[7].

The 3′ terminal segment of PhMV genome encompassing the tymobox-CP–NC sequence (TCN) was specifically PCR amplified using primers,

T1 – GAATTCGAGTCTGAATTGCTTCAC and
N2 – TGGTTTCCGTTACCCACGGAAGGGGGG

from cDNA clone TA51 (ref. 13). The amplified TCN product was gel purified following low melting temperature agarose electrophoresis, end filled and cloned at the *Sma*I site of pBlueScript to obtain the clone pBSTCN[14]. The TCN insert was then released from pBSTCN by *Xba*I/*Hin*dIII double digestion and cloned at the same sites into the binary vector pKYLX 71 35 S^2 (ref. 15) to generate pKYTCN (Figure 1). This binary vector has a duplicated cauliflower mosaic virus 35 S promoter upstream of the multiple cloning site, followed by a ribulose-1,5-bisphosphate carboxylase/oxygenase subunit gene transcription terminator. In addition it also harbours a neomycin phosphotransferase II gene which confers resistance to kanamycin.

pKYTCN was introduced in *Agrobacterium tumefaciens* strain C58C1 by the direct DNA transfer method[16]. Leaf discs of greenhouse-grown *N. tabacum* cv. Havana plants were surface sterilized using standard procedures and

‡For correspondence. (e-mail: bchss@biochem.iisc.ernet.in)

transformed with C58C1 harbouring pKYTCN. The transformed shoots were regenerated on Murashige and Skoog (MS) medium containing vitamins, 0.8% (w/v) agar and 3% (w/v) sucrose supplemented with 1 mg/l 6-benzylaminopurine, 100 mg/l kanamycin and 250 mg/l carbenecillin and were subsequently rooted. Roots were developed on the MS medium supplemented with 1 mg/l indole-3-butyric acid or indole-3-acetic acid, along with 100 mg/l kanamycin and 250 mg/l carbenecillin. The putative transgenic plants in the four-leaf stage were transplanted into pots and used in all the further studies.

Segregation analysis was carried out by germinating the R1 and R2 seeds on plates containing MS medium in the absence or presence of 100 mg/l kanamycin medium. The number of seeds that germinated were counted to evaluate the presence of the transgene.

The transgenic and control plants were mechanically inoculated with either purified virus (10 µg /ml) or PhMV RNA (10 µg/ml) using a sterile glass rod. The appearance of symptoms was monitored on a daily basis until 50 days post inoculation.

Genomic DNA (50 ng) from the control and transformed plants which was isolated by the method of Dellaporta *et al*.[17] was used as template in the PCR reaction. The PCR was performed with CP primers, Ph-N (5′ GCGCCCATGGCCTCCATCCCCGCCCCT 3′) starting with a *Nco*I site (underlined nucleotides) followed by the coding sequences of CP from the 12th amino acid onwards in the sense orientation and Ph-A (5′ CCGGGATCCTTAGTTGGCTATCAG 3′) encompassing the stop codon and a *Bam*HI site (underlined nucleotides) in the antisense orientation. The reaction was carried out using Taq DNA polymerase under the following conditions: 94°C, 1 min for denaturation; 55°C, 1 min for annealing; 72°C, 1 min for elongation (30 cycles). The reaction products were analysed on 1% agarose gel.

Plant genomic DNA samples (25 µg) after restriction digestion with *Eco*RI were analysed on 0.8% agarose gel. The DNA was then transferred to nylon membrane by capillary transfer method and probed with random primer labelled CP gene as described by Sambrook *et al*.[14].

Leaves from transgenic and nontransgenic plants were homogenized in 0.05 M citrate buffer, pH 5.5 and the crude extract (200 µg total protein/well) was subjected to SDS-12% polyacrylamide gel electrophoresis. After electrophoresis the proteins were transferred to a nitrocellulose membrane and Western blot analysis was carried out using the mouse monoclonal antibody PA3B2 to native PhMV as the primary antibody and horseradish peroxidase conjugated goat antimouse IgG as the detecting antibody with 3,3′-diaminobenzidine as the substrate[18].

Empty capsids were isolated from the leaves of transgenic plants following the procedure described earlier for the isolation of top component of PhMV from infected *N. glutinosa* plants[12]. Capsids isolated from control, infected and transgenic plants were loaded onto 10–40% sucrose gradients and centrifuged at 35,000 rpm for 3 h in SW 41 rotor. At the end of the run 0.5 ml fractions were collected and the absorbance was measured at 280 nm. 0.1 mg/ml empty capsids isolated from transgenic plants were applied onto formvar-coated carbon-shadowed copper grids. The particles were visualized by negative staining with 1% (w/v) uranyl acetate and examined by high resolution JEOL 200X electron microscope at a magnification of 68,000 ×.

The pKYTCN construct harbouring the 3′ terminal 748 nucleotides of PhMV genome was obtained as described earlier (Figure 1). The leaf discs of *N. tabacum* cv. Havana plants were transformed with *A. tumefaciens* strain C58C1 harbouring binary vector pKYTCN. A total of 80 putative transformed plants were obtained upon regeneration using the protocol described earlier. Twelve of these plants were found to harbour CP gene by the PCR analysis of DNA isolated from these plants (Figure 2). The remaining plants could be false positives. The reasons for such escapes are unclear. One of these plants (Figure 2, lane 2) did not give a prominent PCR product. Genomic DNA extracted from the

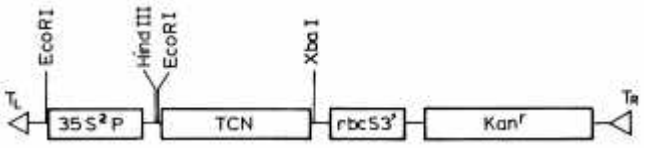

Figure 1. Schematic representation of PhMV sequence in pKYTCN. Duplicated cauliflower mosaic virus 35 S promoter, 3′ end of the gene encoding for the small subunit of ribulose-1,5-bisphosphate carboxylase/ oxygenase (rbcS), Kan^r – neomycin phosphotransferase II gene, T_L and T_R – T-DNA left and right borders, respectively are shown along with the PhMVTCN sequence. The *Xba*I, *Hin*dIII and *Eco*RI sites are indicated by arrows.

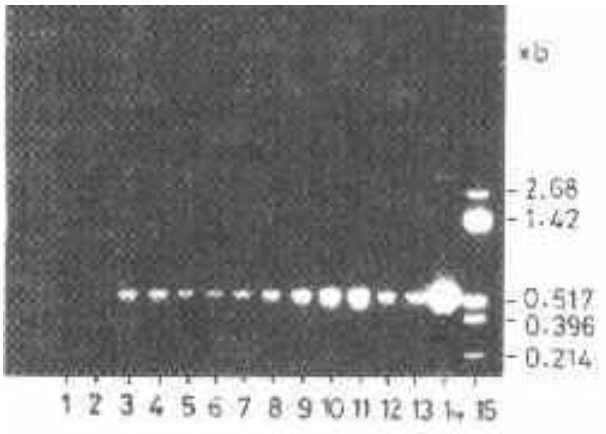

Figure 2. PCR analysis of transgenic plants. 50 ng of genomic DNA extracted from plants were used for PCR amplification with primers corresponding to CP gene. The PCR products were visualized on 1% agarose gel after ethidium bromide staining. Lane 1, nontransgenic plant; lanes 2–13, transgenic plants; lane 14, product obtained when pKYTCN was used as template; lane 15, DNA molecular weight makers.

remaining 11 plants T2–T12 were further subjected to Southern blot analysis (Figure 3). The putative transgenic lines T3–T6 and T8 gave a similar pattern, T9 showed four bands (lane 9) and T2, T7, T11 and T12 gave two bands. No bands were visible in lane 10 corresponding to T10. The similar banding pattern observed in T3–T6 and T8 could be because these putatively transgenic plants were generated from the same explants. Further analysis was carried out with 10 plants T2–T9 and T11–T12 which were confirmed positive by Southern analysis. These plants were transferred to pots and Western blot analysis was performed using the protein extract from the leaves of these plants. All the plants showed similar levels of CP accumulation (Figure 4).

Recombinant PhMV CP expressed in *Escherichia coli* has been shown to self assemble into capsids[19]. In order to examine whether the expressed CP in the transgenic plants was also capable of forming empty capsids, 75 g of leaves pooled from the transgenic R0 plants (shown positive by Southern and Western analysis) and non- transgenic plants were used for isolation of empty capsids formed, if any. A distinct peak co-migrating with the top component (empty capsids formed *in vivo* upon PhMV infection) was seen only in the extracts from transgenic plants and not in the control plants (Figure 5). The inset shows the electron micrograph of the particles isolated from the transgenic plants. Empty capsids of approximately 30 nm diameter with stain penetration in the center could be observed. Similar self-assembly of CPs expressed in transgenic plants has been observed in the case of Norwalk virus[20], TMV[21], arabis mosaic virus[22] and alfalfa mosaic virus (AlMV)[23].

Inoculation of PhMV to *N. tabacum* cv. Havana results in systemic infection leading to severe yellow mottle and leaf distortion within a week. The dilution end point for PhMV (previously named belladonna mottle virus (I)), is 10^{-6} to 10^{-7} (ref. 24). All the 10 R0 plants showed delay in symptom expression while 3 of them showed no detectable symptoms even after 30 days post infection (Figure 6). One of these three R0 plants (T9) which showed no detectable symptoms was self-pollinated and seeds thus formed were used for the production of R1 generation plants. Similarly, one of R1 generation plants that showed no detectable symptom expression upon challenge inoculation with purified virus was self-pollinated and the seeds thus obtained were used for generation of R2 plants. These R1 and R2 seeds (100 each) were germinated in the presence of kanamycin. 80 and 76 out of 100 seeds germinated in the presence of kanamycin in the case of R1 and R2 plants, respectively. The segregation ratio of 3 : 1 is suggestive of the stable integration of transgene and Mendelian pattern of inheritance. R1 and R2 progeny plants (18 each) that were selected on kanamycin medium were allowed to grow and transferred to pots. The total protein was extracted from each of these plants prior to inoculation and Western analysis was performed. It is apparent from Figure 7 *a* and *b* that the level of expression of the CP gene was variable when an equal amount of total protein (200 µg) was loaded from these plants. With the exception of one plant in each group, all of them expressed CP. These groups of 18 R1 and R2 plants which showed the expression of CP were used for evaluation of resistance.

Nine of the R1 and R2 progeny plants along with 9 non transgenic plants were inoculated with 10 µg/ml virus and 10 µg/ml RNA and the symptom expression was monitored over a period of 50 days. As apparent from Tables 1 and 2, all the transgenic plants showed delay in symptom expression. Further, 7 and 2 plants out of 9 R1 and R2 transgenic plants respectively did not show any symptoms even after 50 days post inoculation when inoculated with 10 µg/ml RNA. Similarly, 2 plants out of 9 R1 and R2

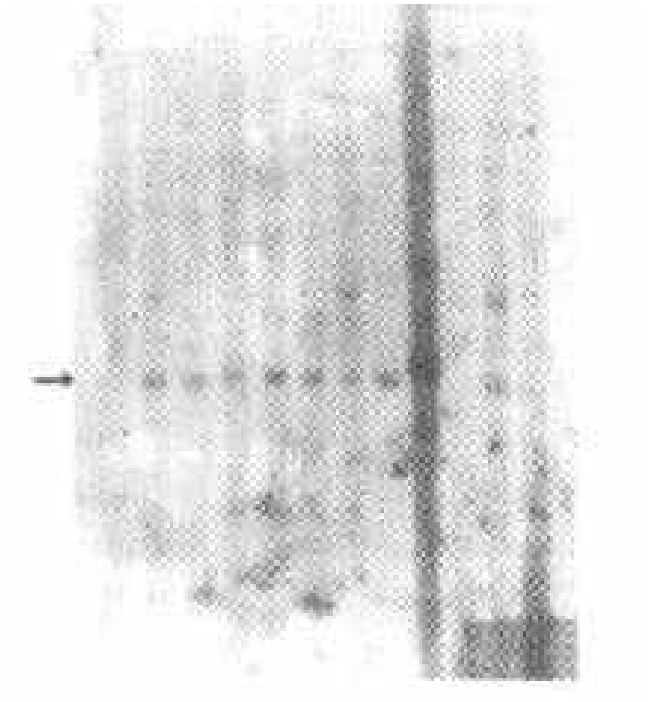

Figure 3. Southern blot analysis of putatively transgenic R0 plants. 25 µg of genomic DNA extracted from plants was digested with *Eco*RI and used for Southern blot analysis with labelled CP gene as probe. Lanes 1 and 13, non-transformed plants. Lanes 2–12, putatively transgenic R0 plants (T2–T12).

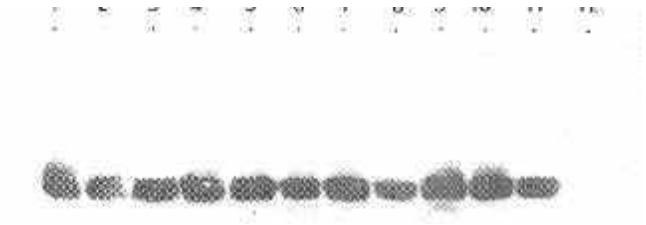

Figure 4. Western blot analysis of R0 transgenic plants. The crude protein extracted from the transgenic R0 plants (1 : 4 w/v) (25 µl) was loaded on SDS 12% PAGE and Western blot analysis was performed using monoclonal antibody PA3B2 against CP as described in text. Lane 1, PhMV control; lanes 2–12, T2–T9 and T11–T12 transgenic plants, and lane 12, non-transgenic plant.

transgenic plants did not show any symptoms 50 days post inoculation with 10 µg/ml virus. 100% infection was observed in all non-transgenic plants on day 4 itself. Interestingly, 4 and 6 of the R1 and R2 plants inoculated with virus showed recovery after 28 days.

The 3′ terminal 748 nucleotides of PhMV genome was introduced into *N. tobaccum* cv Havana plants and the expression of the CP gene was observed in the R0, R1 and R2 transgenic plants. Further, the expressed CP could assemble into capsids *in vivo* (Figure 3). Although the level of expression was similar in the R0 plants it was variable in the R1 and R2 transgenic plants. Further, plants which showed negligible expression exhibited high level of resistance even 30 days after inoculation (example – Figure 7 *a* and *b*, plants 1 and 11 in R1 trangenic plants and plants 5 and 6 in R2 transgenic plants). As evident from Table 1, nearly 80% of the R1 plants inoculated with RNA showed negligible infection. In the group that was challenged with virus, most of the plants showed recovery after 30 days. Thus in the present case, the observed resistance may not be just due to CP-mediated protection. The level of protection was better in the RNA inoculated samples. Even when as high as 10 µg/ml virus was used as inoculum, 2 out of 9 plants showed no detectable symptoms in both R1 and R2 progeny plants from day 1 to day 50. Interestingly, R2 progeny plants seemed to be more susceptible than R1 progeny plants although all of them showed delay in symptom expression. Further, many of the plants which showed mild symptoms also recovered after two months.

The results obtained when the transgenic plants were challenged with genomic viral RNA suggest that inhibition of virus multiplication might have occurred after the uncoating step. The transgenic nucleic acid could compete with the viral genome to redirect host- or viral-encoded

Figure 7. Western analysis of R1 and R2 transgenic plants. ***a***, Equal amount of total protein from each of the plants (200 µg) was loaded and Western analysis carried out using monoclonal antibody PA3B2 against coat protein as described in the text. Lane M, markers (stained with ponceau S and marked as shown prior to Western analysis. Molecular weights are as indicated). Lane H, total protein (200 µg) from control non-transgenic plant. Lanes 1–18 correspond to R1 plants 1–18. ***b***, R2 transgenic plants. Lane M, molecular weight markers; Lane H, non-transgenic control plants; Lanes 1–18 corresponds to R2 transgenic plants 1–18.

Table 1. Disease development in R1 transgenic plants inoculated with PhMV or PhMV RNA

		Disease development during various days post inoculation							
Inoculum	Plant no	4	6	8	10	12	14	28	50
PhMV RNA (10 µg/ml)	1	0	0	0	0	0	0	0	0
	2	0	0	0	0	0	0	0	0
	3	0	0	0	0	0	0	0	0
	4	0	0	0	0	1	1	2	0
	8	0	0	0	0	0	0	0	0
	9	0	0	0	0	0	1	2	2
	13	0	0	0	0	1	2	2	2
	14	0	0	0	0	0	0	0	0
	15	0	0	0	0	0	0	0	0
	C	3	5	5	5	5	5	5	5
PhMV (10 µg/ml)	5	0	0	0	0	1	1	2	0
	6	0	0	0	0	0	0	0	0
	7	0	0	0	0	0	2	2	0
	10	0	0	0	0	0	0	0	0
	11	0	0	0	0	0	0	2	1
	12	0	0	0	0	1	1	2	1
	16	0	0	0	0	0	1	2	1
	17	0	0	0	0	1	1	2	1
	18	0	0	1	1	2	2	3	3
	C	5	5	5	5	5	5	5	5

Figure 5. Sucrose density gradient analysis of virus-like particles in transgenic plants. Capsids were isolated from infected (▲), R0 plants (■) and non-transgenic (●) plants and separated on 10–40% sucrose density gradient. 0.5 ml fractions (from the bottom of the gradient) were collected and the absorbance was monitored at 280 nm. The *y*-axis corresponds to $A_{280\ nm}$ and the *x*-axis corresponds to the fraction number. T, top component (empty capsids), and B, bottom components (intact virus particles). The inset shows the electron micrograph of empty capsids isolated from transgenic plants visualized by negative staining with 1% (w/v) uranyl acetate, at a magnification of 85,000 folds.

Figure 6. Pathogenic manifestation in R0 transgenic plants. The R0 transgenic plants (10 plants) were challenged with 10 µg/ml virus. **1**, Chlorotic lesion hetero-systemic infection. **2**, Chlorotic lesion with mild systemic infection. **3**, Yellow mottling in the newly developing leaves only after inoculation. **4**, Severe systemic yellow mottling with leaf distortion. **C**, Control non-transgenic plants (9 each).

Table 2. Disease development in transgenic R2 plants inoculated with PhMV or PhMV RNA

Inoculum	Plant no	Disease development during various days post inoculation							
		4	6	8	10	12	14	28	50
PhMV RNA (10 μg/ml)	1	0	0	0	0	0	0	0	0
	2	0	0	0	0	1	1	3	3
	3	0	0	0	0	1	1	3	3
	6	0	0	0	0	0	0	0	0
	7	0	0	0	0	1	1	2	1
	8	0	0	0	0	1	1	2	2
	9	0	0	1	1	2	2	3	1
	12	0	0	0	0	1	1	2	2
	13	0	0	0	0	1	1	2	1
	C	3	5	5	5	5	5	5	5
PhMV (10 μg/ml)	4	0	0	0	0	0	0	0	0
	5	0	0	0	0	0	0	0	0
	10	0	0	0	1	1	1	3	1
	11	0	0	0	0	1	1	3	0
	14	0	0	1	1	2	2	3	1
	15	0	0	1	2	2	2	3	1
	16	0	0	0	1	2	2	3	0
	17	0	0	0	0	1	1	2	0
	18	0	0	0	0	0	1	2	0
	C	3	5	5	5	5	5	5	5

0: No sign of infection
1: Chlorotic lesion but no systemic infection
2: Chlorotic lesion with mild systemic infection
3: Yellow mottling in the newly developing leaves only
5: Severe systemic yellow mottling with leaf distortion
C: Control non-transgenic plants (9 each)

proteins into nonproductive interactions for replication or spread of the virus in the infected plant. It was suggested that resistance from a transgenically expressed 3′ noncoding region of TMV RNA was conferred through direct competition with the viral genome[9]. Inhibition of virus multiplication was observed in protoplasts, when they were co-inoculated with PhMV gRNA and transcripts corresponding to 3′ NC region of PhMV[10]. It is possible that even in the whole plant, the RNA transcript encompassing the 3′ NC region might be interfering with the virus multiplication. Similar observations were also made by Yie *et al*.[25] who found elevated resistance to cucumber mosaic virus (CMV) in transgenic tobacco expressing both a CMV CP gene and a satellite RNA of CMV attenuated viral symptom expression. The mechanism of resistance in the present case is not clear and it could be due to the combined effect of expression of CP and 3′ non-coding sequence. Further experiments are in progress to delineate the roles of CP and 3′ NC in conferring resistance to PhMV.

In many of the positive single-stranded RNA plant viruses the CP gene is 3′ proximal. Hence the strategy of using the construct harbouring CP gene and 3′ NC region could be useful in the generation of transgenic plants with elevated levels of resistance against economically important viral diseases.

1. Sanford, J. C. and Johnston, S. A., *J. Theor. Biol.*, 1985, **113**, 395–405.
2. Powell-Abel, P. A., Nelson, R. S., De, B., Hoffmann, N., Rogers, S. G., Fraley, R. T. and Beachy, R. N., *Science*, 1986, **232**, 738–743.
3. Wilson, T. M. A., *Proc. Natl. Acad. Sci. USA*, 1993, **90**, 3134–3141.
4. Lomonossoff, G. P., *Annu. Rev. Phytopathol.*, 1995, **33**, 323–343.
5. Baulcombe, D. C., *Plant Cell.*, 1996, **8**, 1833–1844.
6. Beachy, R. N., *Curr. Opin. Biotechnol.*, 1997, **8**, 215–220.
7. Jacob, A. N. K., Murthy, M. R. N. and Savithri, H. S., *Arch. Virol.*, 1992, **123**, 367–377.
8. Ranjith-Kumar, C. T., Gopinath, K., Jacob, A. N. K., Srividhya, V., Elango, P. and Savithri, H. S., *Arch. Virol.*, 1998, **143**, 1489–1500.
9. Zaccomer, B., Cellier, F., Boyer, J-C., Haenni, A-L. and Tepfer, M., *Gene*, 1993, **136**, 87–94.
10. Ranjith-Kumar, C. T., Haenni, A-L., Savithri, H. S., *J. Gen. Virol.*, 1998, **79**, 185–189.
11. Ding, S., Howe, J., Keese, P., Mackenzie, A., Meek, D., Osorio-Keese, M. O., Skotnicki, M., Srifah, P., Torronen, M. and Gibbs, A., *Nucleic Acid Res.*, 1990, **18**, 1181–1187.
12. Savithri, H. S., Munshi, S. K., Suryanarayana, S., Divakar, S. and Murthy, M. R. N., *J. Gen. Virol.*, 1987, **68**, 1533–1542.
13. Jacob, A. N. K., Ph D thesis, Indian Institute of Science, Bangalore, 1992.
14. Sambrook, J., Fritsch, E. F. and Maniatis, T., *Molecular Cloning –A Laboratory Manual*, Cold Spring Harbor Laboratory Press, New York, 1989.
15. Schardl, C. L., Byrd, A. D., Beuzion, G., Altschuler, M. A., Hildebrand, D. F. and Hunt, A. G., *Gene*, 1987, **61**, 1–11.
16. An, G., *Methods Enzymol.*, 1987, **153**, 292–313.
17. Dellaporta, S. L., Wood, J. and Hicks, J. B., *Plant Mol. Biol. Rep.*, 1983, **1**, 19–21.
18. Kekuda, R., Karande, A. A., Jacob, A. N. K., Savithri, H. S., *Virology*, 1993, **193**, 959–966.
19. Sastri, M., Kekuda, R., Gopinath, K., Ranjith-Kumar, C. T., Jagath, J. R. and Savithri, H. S., *J. Mol. Biol.*, 1997, **272**, 541–552.
20. Mason, H. S., Ball, J. M., Shi, J-J., Jiang, X., Estes, M. K. and Arntzen, C. J., *Proc. Natl. Acad. Sci. USA.*, 1996, **93**, 5335–5340.
21. Clark, W. G., Fitchen, J. H. and Beachy, R. N., *Virology*, 1995, **208**, 485–491.
22. Bertioli, D. J., Harris, R. D., Edwards, M. L., Cooper, J. I. and Hawes, W. S., *J. Gen. Virol.*, 1991, **72**, 1801–1809.
23. Yusibov, V., Modeelska, A., Steplewski, K., Agadjanyan, M., Weiner, D., Hooper, D. C. and Koprowski, H., *Proc. Natl. Acad. Sci. USA*, 1997, **94**, 5784–5788.
24. Moline, H. E. and Fries, R. E., *Phytopathol.*, 1974, **64**, 44–48.
25. Yie, Y., Zhao, F., Zhao, S. Z., Liu, Y. L. and Tien, P., *Mol. Plant-Microbe. Interact.*, 1992, **5**, 460–465.

ACKNOWLEDGEMENTS. We thank Dr A. N. K. Jacob for providing the clone TA 51 and Ms Mira Sastri, Ms Rashmi Talwar, Dr K. Gopinath, Mr Jomon Joseph and Mr B. Venkatesha for help during the course of this study. The help of Dr G. Subbanna in carrying out electron microscopy experiment is gratefully acknowledged. The binary vector pKYLX 71 35 S^2 was a kind gift from Dr M. Tepfer (originally from Dr A. G. Hunt). This work was supported by Department of Biotechnology, India and Indo-French Centre for Promotion of Advanced Research and the Department of Science and Technology, New Delhi, India.

Received 18 August 1999; revised accepted 29 September 1999